AGU PUBLICATIONS

Geophysical Research Letters

RESEARCH LETTER
10.1002/2015GL063737

Key Points:
- Hourly smoke emissions from a wildfire are constrained with multiplatform data
- Diurnal profiles for modeling extreme fire events need to be improved
- Only a multiplatform approach allows to fully resolve emissions for these events

Supporting Information:
- Text S1, Figures S1–S9, and Tables S1–S3

Correspondence to:
P. E. Saide,
pablo-saide@uiowa.edu

Citation:
Saide, P. E., et al. (2015), Revealing important nocturnal and day-to-day variations in fire smoke emissions through a multiplatform inversion, *Geophys. Res. Lett.*, *42*, 3609–3618, doi:10.1002/2015GL063737.

Received 4 MAR 2015
Accepted 19 APR 2015
Accepted article online 22 APR 2015
Published online 13 MAY 2015

Revealing important nocturnal and day-to-day variations in fire smoke emissions through a multiplatform inversion

Pablo E. Saide[1], David A. Peterson[2], Arlindo da Silva[3], Bruce Anderson[4], Luke D. Ziemba[4], Glenn Diskin[4], Glen Sachse[5], Johnathan Hair[4], Carolyn Butler[4], Marta Fenn[4], Jose L. Jimenez[6], Pedro Campuzano-Jost[6], Anne E. Perring[7], Joshua P. Schwarz[7], Milos Z. Markovic[7,8], Phil Russell[9], Jens Redemann[9], Yohei Shinozuka[10,11], David G. Streets[12], Fang Yan[12], Jack Dibb[13], Robert Yokelson[14], O. Brian Toon[15], Edward Hyer[16], and Gregory R. Carmichael[1]

[1]Center for Global and Regional Environmental Research, University of Iowa, Iowa City, Iowa, USA, [2]National Research Council, Monterey, California, USA, [3]NASA Goddard Space Flight Center, Greenbelt, Maryland, USA, [4]NASA Langley Research Center, Hampton, Virginia, USA, [5]National Institute of Aerospace, Hampton, Virginia, USA, [6]Department of Chemistry and Biochemistry, and Cooperative Institute for Research in Environmental Sciences, University of Colorado, Boulder, Colorado, USA, [7]Earth System Research Laboratory, NOAA, Boulder, Colorado, USA, [8]Now at Air Quality Processes Research Section, Environment Canada, Toronto, Ontario, Canada, [9]NASA Ames, Moffett Field, California, USA, [10]NASA Ames Research Center Cooperative for Research in Earth Science and Technology, Moffett Field, California, USA, [11]Bay Area Environmental Research Institute, Petaluma, California, USA, [12]Energy Systems Division, Argonne National Laboratory, Argonne, Illinois, USA, [13]Institute for the Study of Earth, Oceans, and Space, University of New Hampshire, Durham, New Hampshire, USA, [14]Department of Chemistry, University of Montana, Missoula, Montana, USA, [15]Department of Atmospheric and Oceanic Sciences, Laboratory for Atmospheric and Space Physics, University of Colorado, Boulder, Colorado, USA, [16]Marine Meteorology Division, Naval Research Laboratory, Monterey, California, USA

Abstract We couple airborne, ground-based, and satellite observations; conduct regional simulations; and develop and apply an inversion technique to constrain hourly smoke emissions from the Rim Fire, the third largest observed in California, USA. Emissions constrained with multiplatform data show notable nocturnal enhancements (sometimes over a factor of 20), correlate better with daily burned area data, and are a factor of 2–4 higher than a priori estimates, highlighting the need for improved characterization of diurnal profiles and day-to-day variability when modeling extreme fires. Constraining only with satellite data results in smaller enhancements mainly due to missing retrievals near the emissions source, suggesting that top-down emission estimates for these events could be underestimated and a multiplatform approach is required to resolve them. Predictions driven by emissions constrained with multiplatform data present significant variations in downwind air quality and in aerosol feedback on meteorology, emphasizing the need for improved emissions estimates during exceptional events.

1. Introduction

Smoke produced by large-scale biomass burning adversely affects human health, degrades atmospheric visibility, and plays an important role in climate radiative forcing [*Jacobson*, 2014; *Page et al.*, 2002; *Field et al.*, 2009]. Although accurate emission estimates are needed to assess these effects, considerable variability results from the current methodologies [*Feng et al.*, 2014] and modeled smoke predictions usually differ from observations [e.g., *Kaiser et al.*, 2012]. Several studies have constrained smoke emissions on a daily to monthly basis by using a chemical transport model with an optimization algorithm to improve the simulation of observations of atmospheric constituents, which is generally referred to as "inverse modeling." While some of these approaches have assimilated data exclusively from satellite retrievals of gases [*Pfister et al.*, 2005; *Arellano et al.*, 2006; *Kopacz et al.*, 2010], aerosols [*Zhang et al.*, 2005; *Petrenko et al.*, 2012; *Huneeus et al.*, 2012, 2013; *Zhang et al.*, 2014], or both [*Konovalov et al.*, 2014], others have used ground-based measurements [*Cohen and Wang*, 2014; *Mao et al.*, 2014a, 2014b; *Hakami et al.*, 2005]. Although examples of multiplatform inversions for other sources exist [e.g., *Huang et al.*, 2014], there is a growing need for a detailed estimation of wildfire smoke emissions by using multiple observational data sets at high spatial and temporal resolutions [*Hyer et al.*, 2011], as constraints based on single-species measurements are often inconsistent within each other.

Wildfire activity in the western United States has been increasing over the past 3 decades [*Westerling et al.*, 2006]. Several exceptional fire events have also been observed in recent years. One example is the Rim Fire, which affected the central Sierra Nevada Mountains during August–October 2013, becoming the third largest fire in California's history [*Peterson et al.*, 2014]. The Studies of Emissions and Atmospheric Composition, Clouds and Climate Coupling by Regional Surveys (SEAC4RS) field experiment sampled the Rim Fire smoke plume with several instruments onboard the NASA DC-8 aircraft on 26 and 27 August. The combination of airborne, spaceborne, and ground-based observations provides a unique multiplatform data set to characterize the details of the Rim Fire's smoke plume.

This study presents an inverse modeling technique and employs it along with multiplatform observations to constrain hourly Rim Fire smoke emissions, investigate its day-to-day variability, and quantify its diurnal cycle. Model experiments are performed to assess the differences between constrained emissions obtained when assimilating various data sets and to estimate the impacts of these new emissions on air quality simulations, including feedback to local and regional meteorology.

2. Study Region, Methods, and Data

2.1. Regional Modeling

Atmospheric chemistry and aerosol properties were modeled using a modified Carbon Bond Mechanism (CBM-Z) [*Zaveri and Peters*, 1999] and the eight-bin Model for Simulating Aerosol Interactions and Chemistry (MOSAIC) [*Zaveri et al.*, 2008], respectively, within the Weather Research and Forecast with Chemistry (WRF-Chem) coupled chemistry and meteorology regional model [*Skamarock et al.*, 2008; *Grell et al.*, 2005]. Figure 1a shows the domain configuration. While several smoke emission inventories are available, the Quick Fire Emission Dataset (QFED) v2.4 [*Darmenov and da Silva*, 2014; *Petrenko et al.*, 2012] was selected as the a priori estimate because of its skillful performance during SEAC4RS flight planning activities. By employing fire radiative power (FRP) observations from the Moderate Resolution Imaging Spectroradiometer (MODIS), QFED uses FRP-to-emission coefficients adjusted to improve model agreement with aerosol optical depth (AOD) estimates. QFED provided daily biomass burning emissions at 0.1 degree resolution, which were regridded to match the model grids. These emissions were distributed hourly using a diurnal cycle obtained from the Western Regional Air Partnership [*Western Regional Air Partnership*, 2005], which assumes peak emissions during daytime between 17:00–02:00 UTC (10:00–19:00 local time) and low values during the rest of the day and night. Emissions were vertically distributed using the WRF-Chem online plume rise model [*Grell et al.*, 2011], specifying heat-fluxes as in *Freitas et al.* [2007], and a default active fire size of 0.25 km^2. A size distribution representative of fresh forest fire smoke (92% of the mass within 80 to 300 nm dry diameters) was used to partition aerosol emissions into the model size bins, which then produced realistic simulations of the measured Angström exponent, a proxy of the aerosol size distribution (not shown). The application of these temporal, vertical, and size distributions to the QFED emissions is referred to as "initial emissions," which represents the best available a priori knowledge on the source used in the inversion algorithm. Although chemical aging and secondary formation of organic aerosol (OA) can occur in aging smoke plumes, airborne data collected during the Rim Fire showed little change in OA to carbon monoxide (CO) ratio along the length of the plume, which was well represented by the model without secondary OA formation ($<$20% difference for observed CO $<$1000 ppb, observed ratio is noisy for CO $>$1000 ppb). Similar observations have been reported for other fires [*Cubison et al.*, 2011; *Jolleys et al.*, 2012; *Sakamoto et al.*, 2014]; thus, secondary OA processes (which may have occurred on shorter time scales from emission than sampled by the aircraft) were not modeled in our study.

The emission inversion is dependent on the meteorological initial and boundary conditions because variables such as wind speed/direction, temperature, moisture, and boundary layer height greatly influence smoke transport [*Garcia-Menendez et al.*, 2013] and plume rise. This study incorporated National Centers for Environmental Prediction Final Analysis (FNL, http://rda.ucar.edu/datasets/ds083.2/) and North American Regional Reanalysis (NARR, http://rda.ucar.edu/datasets/ds608.0/) in all experiments to test the sensitivity of constrained emissions estimates to meteorology. See Text S1 in the supporting information and section 1 for additional configuration description.

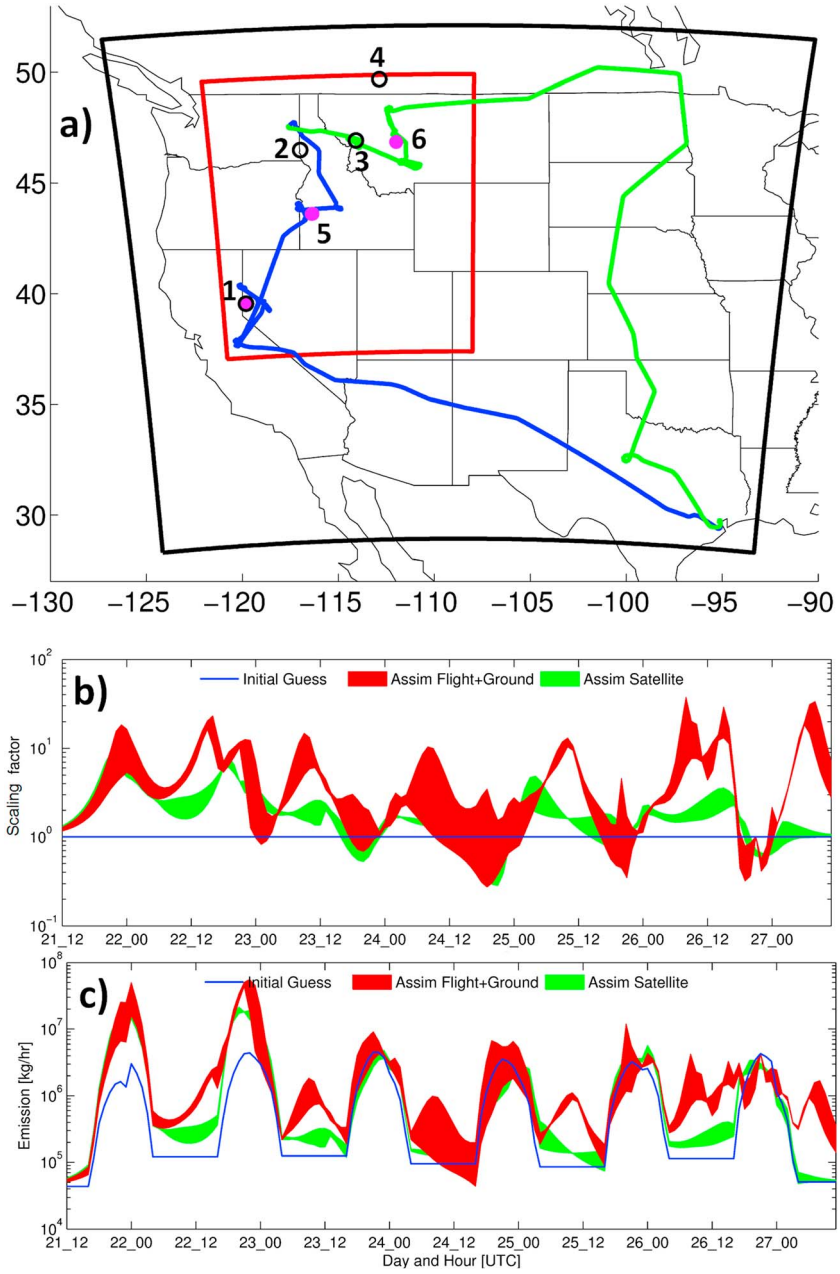

Figure 1. (a) Study region map, with the outer (12 km resolution) and inner (4 km resolution) modeling domains, respectively, displayed in black and red lines, DC-8 flight tracks for 26 and 27 August, respectively, displayed as blue and green lines, AERONET stations displayed as black rings, corresponding to (1) University of Nevada-Reno, (2) Rimrock, (3) Missoula, and (4) University of Lethbridge, and CO stations displayed as magenta circles, corresponding to (1) Reno, (5) Boise (two monitors), and (6) Helena. (b and c) Time series (UTC) of Rim Fire emission scaling factors and CO emissions are, respectively, displayed, with blue solid lines representing the initial estimates. The red and green regions, respectively, represent variability in the constrained estimates when assimilating flight and ground (Flight + Ground) data and only satellite AOD data. The variability, represented by the thickness of the red and green curves, is obtained by performing the inversion when driving the model with different meteorology (see Methods section).

2.2. Inversion Methodology

Simulations with the WRF-Chem model using the full chemistry configuration were performed simultaneously with simulations of source-specific tracers. Each passive tracer corresponds to hourly CO emissions from the Rim Fire region (37.75 to 38.15°N and 120.3 to 119.05°W) for a period of 6 days, starting

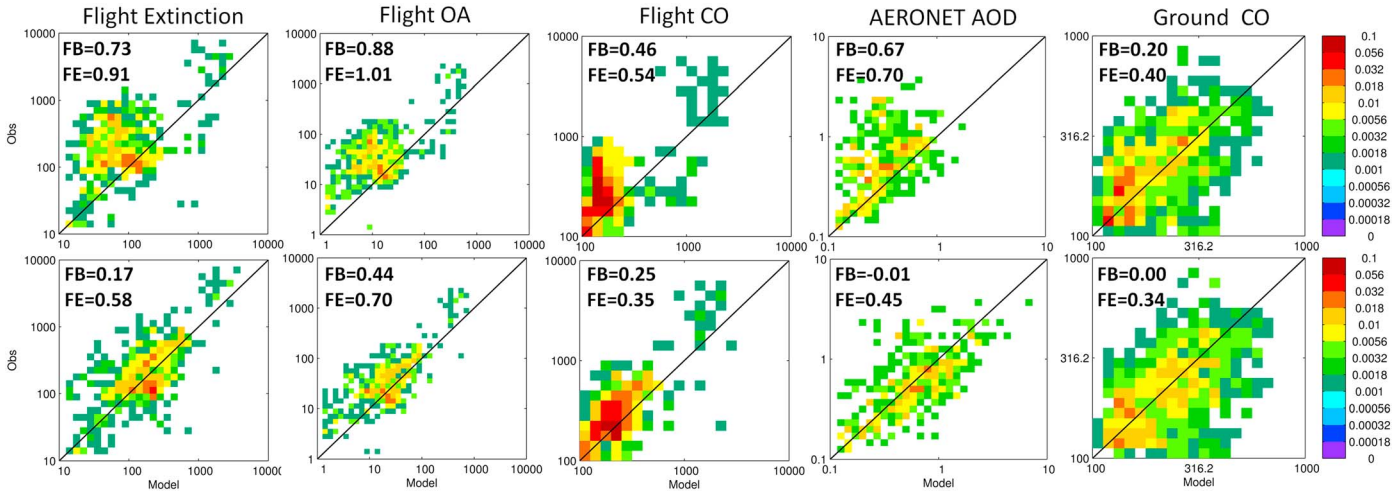

Figure 2. Scatter-density plots depicting the fraction of model and observation pairs in each bin. The columns represent various measurements (extinction (1/Mm), CO (ppb), and AOD), while the top and bottom rows, respectively, correspond to simulations using initial emissions and constrained (Flight + Ground) emissions. Results from simulations using FNL and NARR meteorology are combined in each plot. Fractional bias (FB) and error (FE) with respect to observations (Text S1 in the supporting information and section 4) are provided in each plot.

from the largest fire growth on 21 August (12:00 UTC) up to 27 August (12:00 UTC), thus resulting in 144 tracers. The tracers are then sampled at the observation time/locations.

A total of three simulations for each forcing meteorology were performed: (1) initial emissions, (2) initial emission perturbation (scaled by a factor of 2), and (3) constrained emissions. Simulations (1) and (2) were used to compute finite difference derivatives (i.e., the rate of change of an observable when perturbing emissions) for the hourly CO tracers, which were converted to derivatives of observed variables by using the full-chemistry simulation. These derivatives were used in a variational inverse modeling scheme, which derived the scaling factors applied to hourly Rim Fire emissions. The factors were optimized to generate a better fit to the observations by simultaneously incorporating the a priori knowledge on emissions. See Text S1 in the supporting information and section 2 for a detailed description of the inversion algorithm and derivative computation.

Simulation (3) was performed after the inversion driven by the constrained emissions for investigating the inversion performance (Figure 2) and impacts (Figure 4). Also, the derivatives were recomputed with simulations (1) and (3) (i.e., the perturbation corresponds to the optimized scaling factors) because the derivatives depend on the perturbation due to nonlinearity (Text S1 in the supporting information and section 2). Then, the inversion algorithm was reapplied, and a new set of scaling factors were obtained, which were used in this analysis (Figures 1 and 3). Further iterations were not necessary as the inversion quickly reached convergence (Text S1 in the supporting information and section 2).

The initial emission perturbation and the scaling factors obtained by the inversion were applied to emissions of all chemical and aerosol species within the Rim Fire region. Observed and modeled OA to CO (section 2.1) and black carbon to CO (not shown) ratios strongly agreed for smoke of multiple ages (i.e., along the length of the plume), suggesting that the emission ratios for these species in QFED were close to the observed ratios. Extreme fire behavior prevailed during this period [*Peterson et al.*, 2014], likely producing a flaming-dominant fire both day and night. Thus, not changing emission ratios between species as a function of the stage of the fire (flaming versus smoldering) is a reasonable model approximation. We therefore find it appropriate to simultaneously use aerosol and CO observations for the inversion and to scale aerosol and CO emissions by the same factors. Although we scaled emissions for all chemical and aerosol species, we limit our analysis and conclusions to smoke measurements mentioned in the text.

While this study focuses on a single, large fire event, this approach along with the available observations can also be applied to constrain multiple fires on varying time scales, or extended to other sources (e.g., dust, volcanic emissions, and greenhouse gases). To do so, the appropriate tracers with the desired time resolution and spatial coverage, given the information content in the observations, need to be defined, and the inversion method assumptions and limitations need to be verified. Compared to other inversion

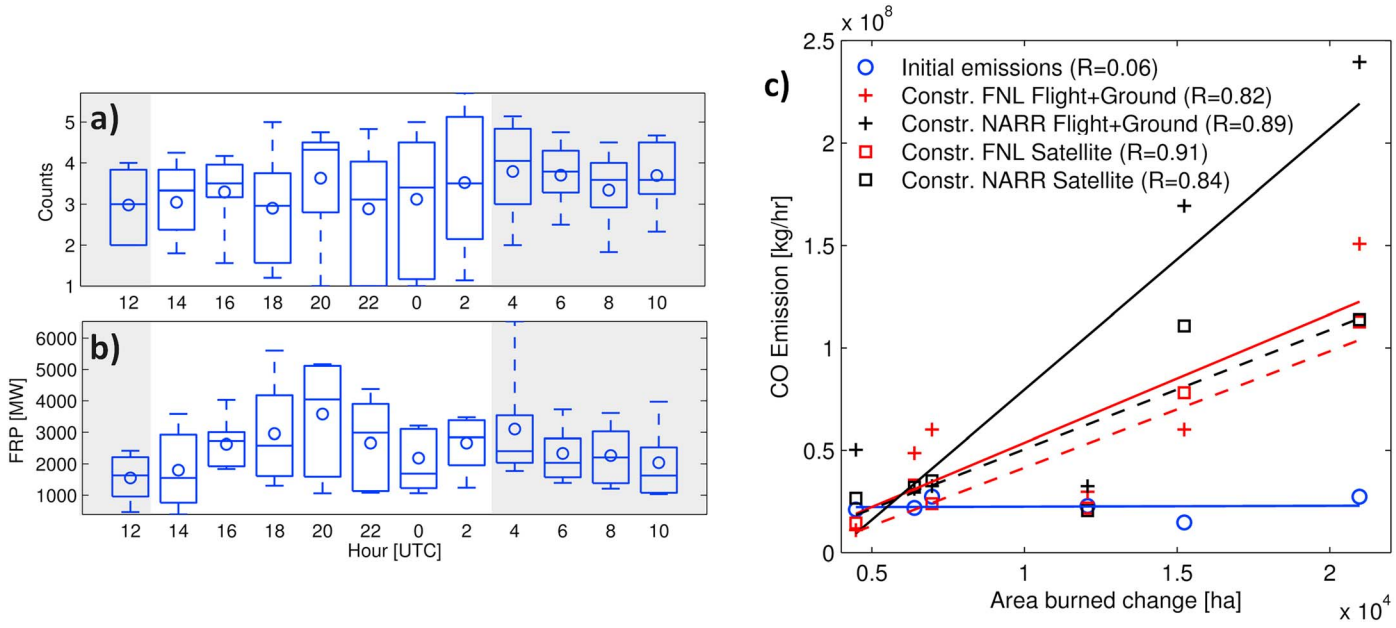

Figure 3. Diurnal cycles of (a) geostationary satellite fire counts and (b) FRP during the study period. The boxes are bounded by the 25th and 75th percentiles, with the median indicated as a line bisecting each box. The whiskers indicate the 10th and 90th percentiles of the data, and the mean values are displayed as open circles. The shaded grey area indicates nighttime. (c) Scatterplots between the change in area burned measured by NIROPS and cumulative emissions over the same time period. The blue circles, red markers, and black markers, respectively, represent initial emissions, constrained emissions using FNL meteorology and constrained emissions using NARR meteorology. The plus and square markers, respectively, represent inversions assimilating Flight + Ground and Satellite data. The solid and dashed lines, respectively, represent regression fit for Flight + Ground and Satellite inversions, with the line color representing the meteorology used. *R* represents the correlation coefficient for each emissions-area set.

algorithms, this method does not require the development of an adjoint, the computational requirements are similar to those of the forward model, and provides emissions fully consistent with WRF-Chem transport (details in Text S1 in the supporting information and section 2).

2.3. Observations

Multiple observational data sets were used simultaneously because the diverse information content provides better constraints on emissions. These observations included AOD and extinction, which capture the accumulation mode smoke burden; OA, which represents the species with the largest contribution to biomass burning aerosol mass (~90% of submicron aerosol for this study); and CO, which is one of the most abundant gases emitted by fires (CO to CO_2 ratio in fresh smoke plumes is ~0.08) and shows large relative increases with respect to background values. We assimilated these data obtained from three types of platforms: airborne, ground-based, and satellite.

Airborne data corresponded to NASA DC-8 measurements of in situ OA [*DeCarlo et al.*, 2006], extinction [*Ziemba et al.*, 2013], and CO [*Sachse et al.*, 1987, 1991], as well as remotely sensed extinction (Figure S1 in the supporting information) [*Hair et al.*, 2008] from flights on 26 and 27 August during the SEAC4RS field experiment. These data provided vertically resolved information of the smoke plume having multiple smoke age along the flight path. The model skillfully represented that the majority of Rim Fire smoke was confined to a deep mixed layer [*Peterson et al.*, 2014] (Figure S1 in the supporting information), allowing airborne data to be used as input for the inversion. Ground-based data corresponded to AOD from the Aerosol Robotic Network (AERONET) [*Holben et al.*, 2001] and CO from air quality networks, which provided daytime constraints of the smoke column and continuous data at the surface, respectively. Both of these data sets increased the temporal coverage of the plume at discrete locations. Finally, satellite AOD retrievals from MODIS provided twice-daily snapshots of AOD with extensive spatial coverage. See details on these and other observations and data selection procedures in Text S1 in the supporting information and section 3.

Two data strategies were used for the inversions: assimilating airborne and ground-based measurements (Flight + Ground) and assimilating only satellite AOD data (satellite only). Explorative inversions (not shown)

presented little deviation in constrained emissions when satellite data were assimilated in addition to Flight + Ground, indicating that the Flight + Ground data set dominates the inversion providing larger information content. Thus, the data strategies selected allow assessing the ability of MODIS satellite data to constrain emissions when additional detailed data are not available and using satellite AOD as an independent data set when validating the Flight + Ground inversion. Four hourly time series of constrained emission sets were obtained by combining the two sets of observations and the two sets of meteorological boundary conditions. Simulation (3) and the update of the scaling factors (see section 2.2) were performed only for Flight + Ground inversions.

The Geostationary Operational Environmental Satellites (GOES) provided the hourly FRP (proxy for fire intensity) and fire counts (fire pixels within the fire perimeter) shown in Figures 3a and 3b. Daily burned area estimates were available from the U.S. Airborne National InfraRed OPerationS (NIROPS, http://nirops.fs.fed.us/).

3. Comparison of Rim Fire Emission Estimates

Assimilating Flight + Ground data results in a factor of 2.7–4.2 increase over the initial emissions during the study period. Underestimations of this magnitude are common when correcting fire emissions across the globe [*Kaiser et al.*, 2012; *Konovalov et al.*, 2014]. Figure 1b shows the time series of hourly scaling factors, which vary from 0.3 to 37. The variability of the factors for each hour (red shading) represents the range of the estimates obtained using the FNL and NARR meteorology. Scaling factors on 24 August show the largest inconsistencies between FNL and NARR experiments, with FNL generally requiring decreased emissions and the NARR requiring increased emissions. This discrepancy is caused by a modeled thick plume being advected over the University of Nevada-Reno AERONET site, producing simulated AOD values larger than 2 with FNL, which is not shown by the observations or by the NARR simulation (Figure S2 in the supporting information). The AOD difference is explained by a slight shift in wind direction between the simulations. Other than this case, hourly scaling factors and emissions (Figure 1c) using FNL and NARR are generally within a factor of 3 and they are highly correlated with each other ($R = 0.83$ for daily emissions). Uncertainties other than the driving meteorology are contributed by specification of inversion parameters and perturbations applied for computing derivatives (Text S1 in the supporting information and section 2). However, after accounting for all these uncertainties, most optimized scaling factors and emissions show similar patterns of increased nighttime activity and higher day-to-day variability, which are analyzed in detail in the following sections.

To evaluate the inversion methodology, model skill using the initial emissions was compared to simulations using Flight + Ground constrained emissions (Figure 2). Results show an improved alignment of data around the 1:1 line after the inversion, indicating closer agreement with extinction, CO, and AERONET AOD observations, which is also reflected by the decrease in fractional bias (FB) and error (FE) ([*Morris et al.*, 2005] also defined in Text S1 in the supporting information and section 4) for all assimilated data sets (in situ OA and remotely sensed extinction in Table S1 in the supporting information). In addition, individual time series of in situ extinction, AERONET AOD, and surface CO show improved performance for simulations using the constrained emissions (Figure S2 in the supporting information). This model evaluation against assimilated data confirms that the inversion method is working properly as it can modify emissions to fit multiple data sets simultaneously. Comparisons between the constrained estimates and other airborne and satellite observations not assimilated (black carbon, sulfate, aerosol number and volume, and airborne and satellite AOD) also show improvements over the initial emissions (satellite AOD in Figure 2, the rest in Table S1 in the supporting information), thus supporting the choice of applying the same scaling factors to all species (section 2.2) and providing an independent validation and showing the robustness of the constrained emissions.

3.1. Diurnal Cycle

Scaling factors are typically higher than 10 during several nighttime periods when assimilating Flight + Ground data (Figures 1b and 1c). This suggests that nocturnal emissions are underestimated in the diurnal cycle assumed by the model (Figure 1c, initial guess). Nocturnal contributions to total daily emissions are 4–8% before the inversion but can reach values as high as 44% after the inversion (Figure 1c). These findings are supported by GOES data, which show persistent fire counts throughout the day and night (Figure 3a), deviating from the typical diurnal cycle of fire activity in the region [*Mu et al.*, 2011].

GOES FRP observations also remain high during the night, but show more of a diurnal cycle than fire counts (Figure 3b). A possible reason for the elevated nocturnal fire activity is the lack of nighttime relative humidity recovery and high nighttime surface wind speeds, driven by the synoptic meteorological pattern during the primary burning period of the Rim Fire [*Peterson et al.*, 2014].

Smoke emissions are usually constrained at daily or longer scales, which require a fixed diurnal cycle that often has little nocturnal fire activity. However, the results shown here indicate that smoke emission estimates and the associated air quality impacts are likely incorrectly estimated during the largest fire events. Therefore, the inclusion of temporally resolved (e.g., hourly) observations of the diurnal cycle of burning [*Zhang et al.*, 2012; *Baldassarre et al.*, 2015] or performing hourly resolved inversions with all available ground-based, airborne and/or satellite data are recommended for simulations of fire events. This has significance beyond large midlatitude fires, as deviations from typical diurnal cycles have also been observed for tropical [*Yokelson et al.*, 2007] and boreal [*Vermote et al.*, 2009] fires.

3.2. Day-to-Day Variability

In contrast to the initial emissions, the emissions constrained by assimilating Flight + Ground data show considerable day-to-day variability (Figure 1c). Similar variability is found in the daily NIROPS burned area estimates as indicated by their strong correlation with the constrained emissions (Figure 3c). Area burned is used in fuel consumption-based inventories as one of several multiplicative factors when estimating emissions [e.g., *Wiedinmyer et al.*, 2011]. Thus, accurate emission estimates should be proportional and highly correlated to an independent and accurate measure of daily area burned (i.e., NIROPS) if fuel-related variables (e.g., biomass loading, fraction of biomass burned, and emission factors) do not change considerably from day to day, i.e., if similar vegetation burned in a similar fashion during the inversion period. This assumption is reasonable as the region that burned was mostly covered by evergreen needleleaf forest, less than 15% of the area was affected by previous fuel treatment [*Johnson et al.*, 2013], and flaming combustion likely predominated due to extreme fire weather conditions [*Peterson et al.*, 2014]. Thus, the proportionality with area burned is another independent test of the robustness of the constrained emissions. The unconstrained initial emissions did not correlate with observed area burned likely because the MODIS FRP retrievals, which provide the day-to-day variability in QFED emissions, were only available four times per day, were obscured during the period of largest fire growth and may have been underestimated as a result of MODIS reaching saturation due to the extent and intensity of the fire (details in Text S1 in the supporting information and section 5). This shows the utility of the inversion method for improving fire emissions estimates.

3.3. Dependence of the Inversion on Observations Assimilated

Total emissions constrained using Satellite-only data (Figure 1c, green area) are 2.1–2.5 times the initial emissions, which is lower than the range of 2.7–4.2 obtained when using Flight + Ground constrained emissions (Figure 1c, red area). This difference can be explained mainly by lower satellite assimilation scaling factors during the night (Figure 1b). AOD retrievals are not possible (or filtered as clouds) for thick smoke plumes, and due to the magnitude of the Rim Fire, valid AOD retrievals were only possible at long distances downwind of the fire after plume dilution had taken place. Measurements far away from the source could be sensitive to a wide temporal range of emissions (e.g., day and night emissions simultaneously) as the footprint of each hourly emission grows with time due to transport and diffusion. This simultaneity favors changes to day-time emissions because they are of higher magnitude and prevents large departures in nocturnal emissions from the initial estimates. In contrast, near-source measurements (e.g., ground-based at Reno, flights close to the source) tend to be sensitive to a narrow temporal range of emissions, which can provide a stronger constraint to nocturnal emissions.

Another explanation for reduced scaling factors from satellite-only data is related to the error introduced after transport within the model. High AOD regions of the plume can be identified in model and satellite data far from the fire, but their geographical location may differ due to errors in model transport. An error in the plume location can prevent a close fit by the assimilation and result in reduced departures from the initial emissions.

The combination of model transport errors and missing near-source AOD retrievals suggests that emissions may be underestimated when constraining smoke emissions from exceptional fire events via satellite AOD

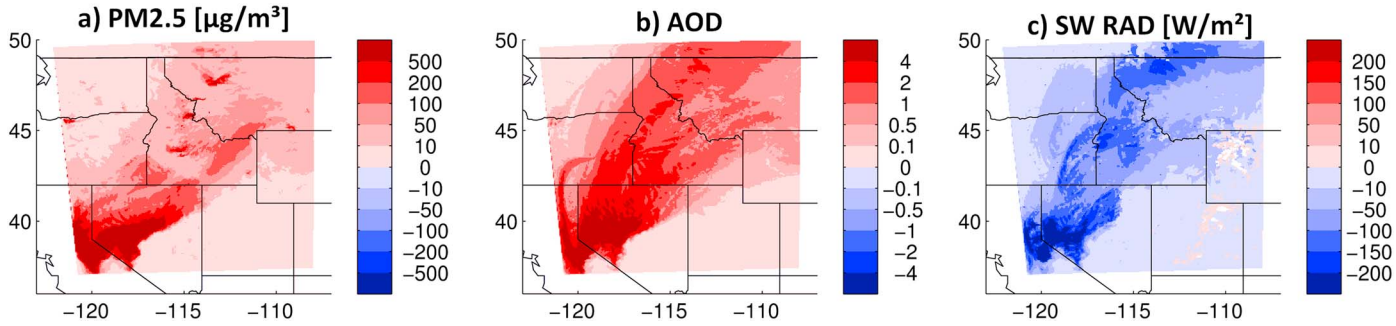

Figure 4. Maps showing the difference of largest magnitude over the entire simulation period between simulations using constrained (Flight + Ground) and initial emissions for surface (a) $PM_{2.5}$, (b) AOD, and clear-sky downward shortwave radiation at the surface (c). These simulations use NARR meteorology.

and that improved characterization can be accomplished using close range measurements. However, in the absence of these measurements, satellite retrievals can still improve the representation of total emissions and of its day-to-day variability, as shown by the high correlation between area burned change and emissions constrained by satellite data (Figure 3c). Future studies should assess impacts of other satellite data such as multispecies (e.g., CO and NH_3 columns) and geo-stationary retrievals.

4. Downwind Impacts

Simulations performed using constrained emissions can substantially modify aerosol loads in the plume with respect to the initial estimates and thus affect air quality predictions (Figure 4a and Figure S2 in the supporting information). Surface particulate pollution is significantly affected in locations such as California and Nevada, which are close to the fire source, with increases in modeled concentration reaching over 500 $\mu g/m^3$ in particulate matter below 2.5 μm in size ($PM_{2.5}$) (Figure 4a). Although the differences decrease as the plume dilutes [e.g., *Feng et al.*, 2014], over 50% of the inner model domain shows increases in $PM_{2.5}$ that reach over 10 $\mu g/m^3$. Improved smoke emissions are not only important for improving forecasts but also for attributing the contribution of fires (versus urban anthropogenic) to air quality degradation, assessing health effects of fires and investigating climate change impacts.

The differences between initial and constrained emission estimates are also pronounced for the column aerosol, with AOD increases reaching values larger than 4 over Nevada and over 0.1 for a large fraction of the domain (Figure 4b). WRF-Chem is a fully coupled online model and thus includes aerosol-radiation interactions [*Fast et al.*, 2006]. As a result, effects on shortwave radiation due to the increase in emissions can also be evaluated (Figure 4c). The additional smoke from the constrained emissions intensifies the dimming of the surface reducing clear-sky downward shortwave radiation by more than 200 W/m^2 across portions of western Nevada, with a large portion of the domain being dimmed by over 10 W/m^2. Changes in radiation balance due to different emissions can affect the local meteorology including temperature and boundary layer height [e.g., *Feng et al.*, 2014] and in combination with aerosol-cloud interactions can have important implications for larger-scale weather phenomena [e.g., *Saide et al.*, 2015].

5. Conclusions

Large-scale biomass burning is increasingly recognized for its adverse effects on air quality, visibility, and health, thus providing motivation for improving smoke emission estimates. By focusing on one of the largest fire events in California's history, this study developed an inversion methodology that uses the WRF-Chem modeling system to constrain hourly smoke emissions. This method differs from the commonly performed inversions that constrain daily (or longer time scale) emissions by constraining hourly emissions using high-resolution (4 km) simulations (full-chemistry and tagged-tracers) driven by initial and perturbed emissions together with a variational inversion framework. The inversion method is able to simultaneously improve the model fit to various SEAC4RS airborne measurements (e.g., OA, CO, and aerosol extinction), ground-based measurements (e.g., AERONET AOD and CO), and satellite data (MODIS AOD) by modifying smoke emissions based on the information content of the combined multiplatform measurements.

Results show that the constrained emissions for a 6 day period including the largest fire growth are a factor 2.7–4.2 higher than the initial emission estimates. Moreover, there is a tendency to increase nocturnal emissions by factors sometimes larger than 20, indicating that vigorous fire activity continued during the night. This deviation from a typical diurnal cycle is confirmed using geostationary satellite data of fire counts and FRP, highlighting the need for modeling with variable emission diurnal profiles during exceptional fire events. The constrained emissions also have a larger day-to-day variability and show stronger correlation with daily area burned estimates based on airborne infrared measurements when compared to the initial emissions. The lower correlation for the initial emissions is due to the MODIS FRP retrievals failing to represent the day-to-day variability of area burned for this event, which encourages the use of inversions to better constrain emissions. Sensitivity experiments with the system show that an inversion based solely on satellite AOD data yields smaller scaling factors than when using all the other data sources. Therefore, emission inversions for exceptional fire events could be underestimated by inversion methods based exclusively on satellite AOD retrievals, which supports current and future deployment of ground-based networks and airborne field experiments along with the use of multispecies data to study fires. Variations in smoke emissions can have a significant impact on surface air quality, aerosol load, and its effects on local and regional meteorology, highlighting the need for performing these studies.

Acknowledgments

We thank all SEAC4RS participants that made the field experiment possible, especially Project Manager Hal Maring. We also thank Brent Holben, Patrick Arnott, Min Hao, Craig Coburn, Adriana Predoi-Cross, and their staff for establishing and maintaining the AERONET sites used in this investigation. This work was carried out with the aid of NSF grant 1049140 NCE; NASA grants NNX11AI52G, NNH12AT27i, NNX12AC03G, NNX12AC20G, and NNX12AC64G; EPA grant 83503701; and grant number UL1RR024979 from the National Center for Research Resources, a part of the National Institutes of Health. Its contents are solely the responsibility of the authors and do not necessarily represent the official views of the funding institutions. Contact P. E. Saide (pablo-saide@uiowa.edu) or G. R. Carmichael (gregory-carmichael@uiowa.edu) for data requests.

The Editor thanks Avelino Arellano and two anonymous reviewers for their assistance in evaluating this paper.

References

Arellano, A. F., P. S. Kasibhatla, L. Giglio, G. R. van der Werf, J. T. Randerson, and G. J. Collatz (2006), Time-dependent inversion estimates of global biomass-burning CO emissions using Measurement of Pollution in the Troposphere (MOPITT) measurements, *J. Geophys. Res.*, *111*, D09303, doi:10.1029/2005JD006613.

Baldassarre, G., L. Pozzoli, C. C. Schmidt, A. Unal, T. Kindap, W. P. Menzel, S. Whitburn, P. F. Coheur, A. Kavgaci, and J. W. Kaiser (2015), Using SEVIRI fire observations to drive smoke plumes in the CMAQ air quality model: The case of Antalya in 2008, *Atmos. Chem. Phys. Discuss.*, *15*, 1–46, doi:10.5194/acpd-15-1-2015.

Cohen, J. B., and C. Wang (2014), Estimating global black carbon emissions using a top-down Kalman Filter approach, *J. Geophys. Res. Atmos.*, *119*, 307–323, doi:10.1002/2013JD019912.

Cubison, M. J., et al. (2011), Effects of aging on organic aerosol from open biomass burning smoke in aircraft and laboratory studies, *Atmos. Chem. Phys.*, *11*, 12,049–12,064, doi:10.5194/acp-11-12049-2011.

Darmenov, A., and A. M. da Silva (2014), The Quick Fire Emissions Dataset (QFED)—Documentation of versions 2.1, 2.2 and 2.4, NASA TM-2013-104606, vol. 35, 183 pp. [Available at http://gmao.gsfc.nasa.gov/pubs/tm/].

DeCarlo, P. F., et al. (2006), Field-deployable, high-resolution, time-of-flight aerosol mass spectrometer, *Anal. Chem.*, *78*, 8281–8289, doi:10.1021/ac061249n.

Fast, J. D., W. I. Gustafson Jr., R. C. Easter, R. A. Zaveri, J. C. Barnard, E. G. Chapman, G. A. Grell, and S. E. Peckham (2006), Evolution of ozone, particulates, and aerosol direct radiative forcing in the vicinity of Houston using a fully coupled meteorology-chemistry-aerosol model, *J. Geophys. Res.*, *111*, D21305, doi:10.1029/2005JD006721.

Feng, Z., et al. (2014), Sensitivity of mesoscale modeling of smoke direct radiative effect to the emission inventory: A case study in northern sub-Saharan African region, *Environ. Res. Lett.*, *9*, 075002.

Field, R. D., G. R. van der Werf, and S. S. P. Shen (2009), Human amplification of drought-induced biomass burning in Indonesia since 1960, *Nat. Geosci.*, *2*, 185–188. [Available at http://www.nature.com/ngeo/journal/v2/n3/suppinfo/ngeo443_S1.html.]

Freitas, S. R., K. M. Longo, R. Chatfield, D. Latham, M. A. F. Silva Dias, M. O. Andreae, E. Prins, J. C. Santos, R. Gielow, and J. A. Carvalho Jr. (2007), Including the sub-grid scale plume rise of vegetation fires in low resolution atmospheric transport models, *Atmos. Chem. Phys.*, *7*, 3385–3398, doi:10.5194/acp-7-3385-2007.

Garcia-Menendez, F., Y. Hu, and M. T. Odman (2013), Simulating smoke transport from wildland fires with a regional-scale air quality model: Sensitivity to uncertain wind fields, *J. Geophys. Res. Atmos.*, *118*, 6493–6504, doi:10.1002/jgrd.50524.

Grell, G., S. E. Peckham, R. Schmitz, S. A. McKeen, G. Frost, W. C. Skamarock, and B. Eder (2005), Fully coupled "online" chemistry within the WRF model, *Atmos. Environ.*, *39*, 6957–6975, doi:10.1016/j.atmosenv.2005.04.027.

Grell, G., S. R. Freitas, M. Stuefer, and J. Fast (2011), Inclusion of biomass burning in WRF-Chem: Impact of wildfires on weather forecasts, *Atmos. Chem. Phys.*, *11*, 5289–5303, doi:10.5194/acp-11-5289-2011.

Hair, J. W., C. A. Hostetler, A. L. Cook, D. B. Harper, R. A. Ferrare, T. L. Mack, W. Welch, L. R. Izquierdo, and F. E. Hovis (2008), Airborne high spectral resolution lidar for profiling aerosol optical properties, *Appl. Opt.*, *47*, 6734–6752, doi:10.1364/ao.47.006734.

Hakami, A., D. Henze, J. Seinfeld, T. Chai, Y. Tang, G. Carmichael, and A. Sandu (2005), Adjoint inverse modeling of black carbon during the Asian Pacific Regional Aerosol Characterization Experiment, *J. Geophys. Res.*, *110*, D14301, doi:10.1029/2004JD005671.

Holben, B., D. Tanré, A. Smirnov, T. Eck, I. Slutsker, N. Abuhassan, W. Newcomb, J. Schafer, B. Chatenet, and F. Lavenu (2001), An emerging ground-based aerosol climatology: Aerosol optical depth from AERONET, *J. Geophys. Res.*, *106*, 12,067–12,097, doi:10.1029/2001JD900014.

Huang, M., et al. (2014), Changes in nitrogen oxides emissions in California during 2005–2010 indicated from top-down and bottom-up emission estimates, *J. Geophys. Res. Atmos.*, *119*, 12,928–12,952, doi:10.1002/2014JD022268.

Huneeus, N., F. Chevallier, and O. Boucher (2012), Estimating aerosol emissions by assimilating observed aerosol optical depth in a global aerosol model, *Atmos. Chem. Phys.*, *12*, 4585–4606, doi:10.5194/acp-12-4585-2012.

Huneeus, N., O. Boucher, and F. Chevallier (2013), Atmospheric inversion of SO2 and primary aerosol emissions for the year 2010, *Atmos. Chem. Phys.*, *13*, 6555–6573, doi:10.5194/acp-13-6555-2013.

Hyer, E., J. Wang, and A. Arellano (2011), Biomass burning: Observations, modeling, and data assimilation, *Bull. Am. Meteorol. Soc.*, *93*, ES10–ES14, doi:10.1175/bams-d-11-00064.1.

Jacobson, M. Z. (2014), Effects of biomass burning on climate, accounting for heat and moisture fluxes, black and brown carbon, and cloud absorption effects, *J. Geophys. Res. Atmos.*, 8980–9002, doi:10.1002/2014JD021861.

Johnson, M., S. Crook, M. Stuart, and M. Romero (2013), Rim Fire—Preliminary Fuel Treatment Effectiveness Report, pp. 7. [Available at http://www.fs.usda.gov/Internet/FSE_DOCUMENTS/stelprdb5436551.pdf.]
Jolleys, M. D., et al. (2012), Characterizing the aging of biomass burning organic aerosol by use of mixing ratios: A meta-analysis of four regions, *Environ. Sci. Technol.*, *46*, 13,093–13,102, doi:10.1021/es302386v.
Kaiser, J. W., et al. (2012), Biomass burning emissions estimated with a global fire assimilation system based on observed fire radiative power, *Biogeosciences*, *9*, 527–554, doi:10.5194/bg-9-527-2012.
Konovalov, I. B., et al. (2014), Constraining CO2 emissions from open biomass burning by satellite observations of co-emitted species: A method and its application to wildfires in Siberia, *Atmos. Chem. Phys.*, *14*, 10,383–10,410, doi:10.5194/acp-14-10383-2014.
Kopacz, M., et al. (2010), Global estimates of CO sources with high resolution by adjoint inversion of multiple satellite datasets (MOPITT, AIRS, SCIAMACHY, TES), *Atmos. Chem. Phys.*, *10*, 855–876, doi:10.5194/acp-10-855-2010.
Mao, Y. H., Q. B. Li, D. Chen, L. Zhang, W. M. Hao, and K. N. Liou (2014a), Top-down estimates of biomass burning emissions of black carbon in the Western United States, *Atmos. Chem. Phys.*, *14*, 7195–7211, doi:10.5194/acp-14-7195-2014.
Mao, Y. H., et al. (2014b), Variational estimates of black carbon emissions in the western United States, *Atmos. Chem. Phys. Discuss.*, *14*, 21,865–21,916, doi:10.5194/acpd-14-21865-2014.
Morris, R. E., D. E. McNally, T. W. Tesche, G. Tonnesen, J. W. Boylan, and P. Brewer (2005), Preliminary evaluation of the Community Multiscale Air Quality model for 2002 over the southeastern United States, *J. Air Waste Manage.*, *55*, 1694–1708.
Mu, M., et al. (2011), Daily and 3-hourly variability in global fire emissions and consequences for atmospheric model predictions of carbon monoxide, *J. Geophys. Res.*, *116*, D24303, doi:10.1029/2011JD016245.
Page, S. E., F. Siegert, J. O. Rieley, H.-D. V. Boehm, A. Jaya, and S. Limin (2002), The amount of carbon released from peat and forest fires in Indonesia during 1997, *Nature*, *420*, 61–65.
Peterson, D. A., E. J. Hyer, J. R. Campbell, M. D. Fromm, J. W. Hair, C. F. Butler, and M. A. Fenn (2014), The 2013 Rim Fire: Implications for predicting extreme fire spread, pyroconvection, and smoke emissions, *Bull. Am. Meteorol. Soc.*, *96*, 229–247, doi:10.1175/bams-d-14-00060.1.
Petrenko, M., R. Kahn, M. Chin, A. Soja, T. Kucsera, and Harshvardhan (2012), The use of satellite-measured aerosol optical depth to constrain biomass burning emissions source strength in the global model GOCART, *J. Geophys. Res.*, *117*, D18212, doi:10.1029/2012JD017870.
Pfister, G., P. G. Hess, L. K. Emmons, J. F. Lamarque, C. Wiedinmyer, D. P. Edwards, G. Pétron, J. C. Gille, and G. W. Sachse (2005), Quantifying CO emissions from the 2004 Alaskan wildfires using MOPITT CO data, *Geophys. Res. Lett.*, *32*, L11809, doi:10.1029/2005GL022995.
Sachse, G. W., G. F. Hill, L. O. Wade, and M. G. Perry (1987), Fast-response, high-precision carbon monoxide sensor using a tunable diode laser absorption technique, *J. Geophys. Res.*, *92*, 2071–2081, doi:10.1029/JD092iD02p02071.
Sachse, G. W., J. J. E. Collins, G. F. Hill, L. O. Wade, L. G. Burney, and J. A. Ritter (1991), Airborne tunable diode laser sensor for high-precision concentration and flux measurements of carbon monoxide and methane, *Proc. SPIE*, *1433*, 157–166, doi:10.1117/12.46162.
Saide, P. E., S. N. Spak, R. B. Pierce, J. A. Otkin, T. K. Schaack, A. K. Heidinger, A. M. da Silva, M. Kacenelenbogen, J. Redemann, and G. R. Carmichael (2015), Central American biomass burning smoke can increase tornado severity in the U.S., Geophys. *Res. Lett.*, *42*, 956–965, doi:10.1002/2014GL062826.
Sakamoto, K. M., J. D. Allan, H. Coe, J. W. Taylor, T. J. Duck, and J. R. Pierce (2014), Aged boreal biomass burning aerosol size distributions from BORTAS 2011, *Atmos. Chem. Phys. Discuss.*, *14*, 24,349–24,385, doi:10.5194/acpd-14-24349-2014.
Skamarock, W. C., J. B. Klemp, J. Dudhia, D. O. Gill, D. M. Barker, M. G. Duda, X.-Y. Huang, W. Wang, and J. G. Powers (2008), A description of the Advanced Research WRF version 3, *NCAR Tech. Note NCAR/TN-475+ STR*.
Vermote, E., E. Ellicott, O. Dubovik, T. Lapyonok, M. Chin, L. Giglio, and G. J. Roberts (2009), An approach to estimate global biomass burning emissions of organic and black carbon from MODIS fire radiative power, *J. Geophys. Res.*, *114*, D18205, doi:10.1029/2008JD011188.
Westerling, A. L., H. G. Hidalgo, D. R. Cayan, and T. W. Swetnam (2006), Warming and earlier spring increase western U.S. forest wildfire activity, *Science*, *313*, 940–943, doi:10.1126/science.1128834.
Western Regional Air Partnership (2005), 2002 Fire Emission Inventory for the WRAP Region- Phase II, Project No. 178–6. [Available at http://www.wrapair.org/forums/fejf/tasks/FEJFtask7PhaseII.html.]
Wiedinmyer, C., S. K. Akagi, R. J. Yokelson, L. K. Emmons, J. A. Al-Saadi, J. J. Orlando, and A. J. Soja (2011), The Fire INventory from NCAR (FINN): A high resolution global model to estimate the emissions from open burning, *Geosci. Model Dev.*, *4*, 625–641, doi:10.5194/gmd-4-625-2011.
Yokelson, R. J., T. Karl, P. Artaxo, D. R. Blake, T. J. Christian, D. W. T. Griffith, A. Guenther, and W. M. Hao (2007), The tropical forest and fire emissions experiment: Overview and airborne fire emission factor measurements, *Atmos. Chem. Phys.*, *7*, 5175–5196, doi:10.5194/acp-7-5175-2007.
Zaveri, R. A., and L. K. Peters (1999), A new lumped structure photochemical mechanism for large-scale applications, *J. Geophys. Res.*, *104*, 30,387–30,415, doi:10.1029/1999JD900876.
Zaveri, R. A., R. C. Easter, J. D. Fast, and L. K. Peters (2008), Model for Simulating Aerosol Interactions and Chemistry (MOSAIC), *J. Geophys. Res.*, *113*, D13204, doi:10.1029/2007JD008782.
Zhang, L., D. K. Henze, G. A. Grell, G. R. Carmichael, N. Bousserez, Q. Zhang, and J. Cao (2014), Constraining black carbon aerosol over Southeast Asia using OMI aerosol absorption optical depth and the adjoint of GEOS-Chem, *Atmos. Chem. Phys. Discuss.*, *14*, 28,385–28,452, doi:10.5194/acpd-14-28385-2014.
Zhang, S., J. E. Penner, and O. Torres (2005), Inverse modeling of biomass burning emissions using Total Ozone Mapping Spectrometer aerosol index for 1997, *J. Geophys. Res.*, *110*, D21306, doi:10.1029/2004JD005738.
Zhang, X., S. Kondragunta, J. Ram, C. Schmidt, and H.-C. Huang (2012), Near-real-time global biomass burning emissions product from geostationary satellite constellation, *J. Geophys. Res.*, *117*, D14201, doi:10.1029/2012JD017459.
Ziemba, L. D., et al. (2013), Airborne observations of aerosol extinction by in situ and remote-sensing techniques: Evaluation of particle hygroscopicity, *Geophys. Res. Lett.*, *40*, 417–422, doi:10.1029/2012GL054428.